International Journal of
Molecular Sciences

MDPI

Article

Multi-Omics Profiles Reveal Molecular Regulation of Ovarian Aging in Chickens

Wenao Ma [1,2], Axiu Guo [1,2], Siyu Huang [1,2], Wenhui Zhang [1,2], Hongliang Zhang [3], Hao Zhang [1,2] and Bo Zhang [1,2,*]

[1] Frontiers Science Center for Molecular Design Breeding (MOE), China Agricultural University, Bejing 100193, China; 13281001183@163.com (W.M.); guoaxiu12139@163.com (A.G.); hsy08262002@163.com (S.H.); b20213040327@cau.edu.cn (W.Z.); hzhang@cau.edu.cn (H.Z.)
[2] National Engineering Laboratory for Animal Breeding, Beijing Key Laboratory for Animal Genetic Improvement, College of Animal Science and Technology, China Agricultural University, Beijing 100193, China
[3] Department of Animal Husbandry, Xizang Agricultural and Animal Husbandry University, Linzhi 860000, China; holiangzhang@126.com
* Correspondence: bozhang0606@cau.edu.cn; Tel.: +86-18211192479

Abstract

Ovarian aging shortens the laying cycle in hens, thereby reducing egg production and posing a major constraint on the economic efficiency and sustainability of the poultry industry. This study integrates three omics approaches to investigate the molecular alterations underlying age-related ovarian functional decline. We employed an integrated approach combining RNA sequencing (RNA-seq), ribosome profiling (Ribo-seq), and data-independent acquisition (DIA) proteomics, with selected targets validated by qRT-PCR and Western blotting. Ovarian tissues with follicles > 8 mm removed were collected from a total of 12 hens, including six 30-week-old hens (W30, $n = 6$) and six 90-week-old hens (W90, $n = 6$), to identify age-associated changes in gene expression, ribosome footprints (RFs), and protein abundance. A total of 18,836 genes, 17,007 RFs, and 6738 proteins were detected. Among these, 562 genes, 430 genes with altered translation efficiency (TE), and 252 proteins were differentially expressed between the two groups. Further analyses indicated that, in aged ovaries, the down-regulation of steroidogenic genes, including *STAR*, *CYP11A1*, *HSD3B1*, and *FDX1*, was associated with reduced steroid hormone synthesis. The up-regulation of matrix stiffness-related proteins, including MFAP4 and SGCE, together with the down-regulation of genes and proteins associated with matrix degradation and autophagic clearance, including *ADAMTS15*, *MRC1*, RAB7A, and CTSB, was indicative of ovarian tissue sclerosis. In summary, the multi-omics data revealed that ovarian aging in laying hens is associated with coordinated alterations across multiple molecular layers. This study identifies key genes and proteins associated with ovarian aging and provides a foundation for generating mechanistic hypotheses regarding the molecular processes involved.

Keywords: laying hen; ovarian aging; translation efficiency; multi-omics

Check for updates

Academic Editor: Mahmoud Mostafa Azzam

Received: 19 October 2026
Revised: 16 November 2026
Accepted: 18 November 2026
Published: 19 November 2026

Copyright: © 2026 by the authors. Licensee MDPI, Basel, Switzerland. This article is an open access article distributed under the terms and conditions of the Creative Commons Attribution (CC BY) license.

1. Introduction

Ovarian aging in mammals has been extensively investigated and is typically characterized by depletion of the follicular reserve, reduced oocyte quality, and other age-related alterations. Recent single-cell transcriptomic, spatial transcriptomic, and multi-omics studies

in humans, non-human primates, mice, and livestock species have revealed multiple regulatory mechanisms underlying ovarian aging, including oxidative stress, DNA damage, cellular senescence, epigenetic remodeling, tissue fibrosis, and increased tissue stiffness [1–4]. Although these studies provide valuable references for poultry research, substantial differences in reproductive physiology and ovulatory patterns between mammals and poultry necessitate targeted investigation of ovarian aging in poultry.

White Leghorn chickens trace their ancestry to chickens from the Livorno area of central Italy. After being exported to the United States and Britain, these chickens were developed by breeders into the modern White Leghorn. They are one of the most widely raised egg-type chicken breeds in China and worldwide due to their early sexual maturity, high egg production and low feed consumption [5]. As high-producing layers, they require sustained and stable ovarian function. The ovary is the organ that controls egg production by orchestrating follicular development, yolk deposition and ovulation [6,7]. However, overt signs of aging appear in the ovary earlier and progress more rapidly than in any other organ [8]. As the chickens age, ovarian dysfunction leads to the dysregulation of reproductive hormones and the accumulation of oxidative stress. This suppresses follicular growth, reduces the number of follicles at all developmental stages and increases follicular atresia. These changes manifest as prolonged laying intervals and a higher incidence of soft-shelled and misshapen eggs [9,10]. Additionally, hatchability and chick quality from breeder hens in the late laying period decline [11]. Although research into the regulation of ovarian function has intensified, studies focusing on hens transitioning from the peak egg-laying period to the late egg-laying period remain limited. The factors contributing to ovarian aging and their underlying mechanisms have not yet been fully elucidated. Investigating differences in ovarian status and regulatory factors between peak and late egg-laying stages is significant for improving egg production performance in poultry breeding.

In recent years, advances in high-throughput sequencing and mass spectrometry have led to their widespread application. Transcriptomics can provide regulatory information at the gene level [12], while proteomics reveals regulatory mechanisms at the protein level [13]. However, the flow of genetic information from mRNA to protein is regulated at multiple levels, including transcription, post-transcription, translation, and post-translation. These multilayered regulatory processes result in a relatively weak correlation between transcriptomic and proteomic data, making it difficult to elucidate the functions and regulatory pathways of genes and proteins using either approach alone [14]. Translational control is a particularly critical regulatory layer in living organisms and investigating translational regulation is becoming increasingly necessary [15]. Currently, integrated analyses combining translatomics with transcriptomics, proteomics, and other 'omics' are powerful tools for dissecting the molecular mechanisms of biological processes. For instance, combined transcriptomic and translatomic approaches have been adopted in previous studies to identify and screen key genes governing sperm storage capacity in laying hens [16]. Huang et al. [17] revealed that the YTH domain-containing protein 3 (YTHDF3) plays a pivotal role in oocyte aging in mice by integrating translatomics, proteomics, and transcriptomics.

In this study, we conducted an integrated analysis of transcriptome, translatome and proteome data alongside phenotypic traits, investigating the molecular mechanisms underlying ovarian aging in white leghorn hens. Our findings enhance our understanding of ovarian aging in laying hens and could inform strategies to extend the productive laying period, maintain egg-laying rates, and improve economic efficiency in the poultry industry.

2. Results

2.1. Ovarian Characteristics

In this study, the numbers of 6–8 mm follicles and follicles > 9 mm in W90 hens were significantly lower than those in W30 hens (Table 1 and Supplementary Figure S1). Hematoxylin and eosin (H&E)-stained ovarian sections were used to examine ovarian morphology, and follicles were evaluated according to their diameter and morphological characteristics. In W30 ovaries, follicles at different developmental stages were densely distributed, with abundant follicles present throughout the ovarian stroma. The ovarian surface appeared swollen and protuberant, and some follicles showed signs of atresia (Figure 1A–C). In contrast, follicles at all developmental stages were markedly sparser in W90 ovaries. The ovarian stroma of W90 hens was predominantly populated by follicles ≤ 0.08 mm in diameter, whereas follicles measuring 1–3 mm were relatively scarce. Atretic follicles were also observed (Figure 1D–F).

Table 1. Statistics of body weight, ovarian weight and follicle counts in W30 and W90 hens.

Parameter	W30	W90	*p*-Value
Body weight (g)	1436.67 ± 206.56	1584.38 ± 201.07	0.2400
Ovary weight (g)	52.37 ± 10.87	43.17 ± 7.02	0.1121
follicle weight (g)	48.41 ± 10.42	39.48 ± 6.72	0.1082
Ovary weight/BW	0.04 ± 0.01	0.03 ± 0.01	0.0018
3–5 mm follicles (count)	23.00 ± 4.05	18.17 ± 4.92	0.0930
6–8 mm follicles (count)	10.67 ± 3.39	6.17 ± 3.31	0.0420
Follicles > 9 mm (count)	6.83 ± 0.98	5.33 ± 0.52	0.0079

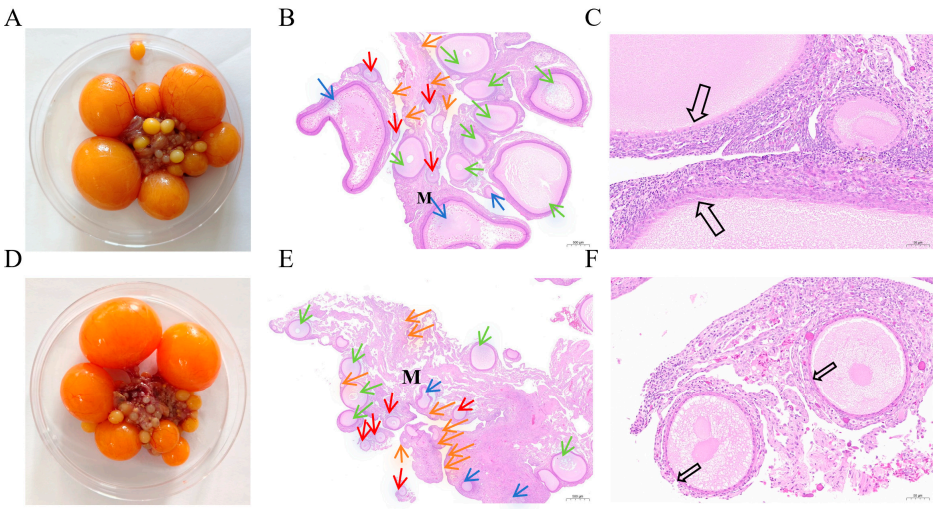


Figure 1. Morphological characteristics of ovaries at different laying stages. (**A**) Ovaries from W30 hens. (**B**,**C**) H&E-stained ovarian sections from W30 hens. (**D**) Ovaries from W90 hens. (**E**,**F**) H&E-stained ovarian sections from W90 hens. Yellow arrows: primordial follicles (≤0.08 mm); M: ovarian medulla; red arrows: primary follicles (0.08–1 mm); green arrows: fast-growing secondary follicles (1–3 mm); blue arrows: atretic follicles (AF); Black arrow: granulosa cell layer within the follicle.

2.2. Transcriptome Analysis

The transcriptomic results of this study yielded a total of 42.44 to 48.22 million cleaned RNA-seq reads, with reference genome alignment rates ranging from 92.60% to 93.40%. It was established that both sample consistency and gene expression distribution satisfied the requisite standard quality control metrics (Supplementary Table S1). These findings indicate satisfactory sequencing outcomes suitable for subsequent analysis. Among the

18, 836 detected genes, 562 DEGs were identified, comprising 352 down-regulated and 210 up-regulated genes in W90 relative to W30 (Figure 2A).

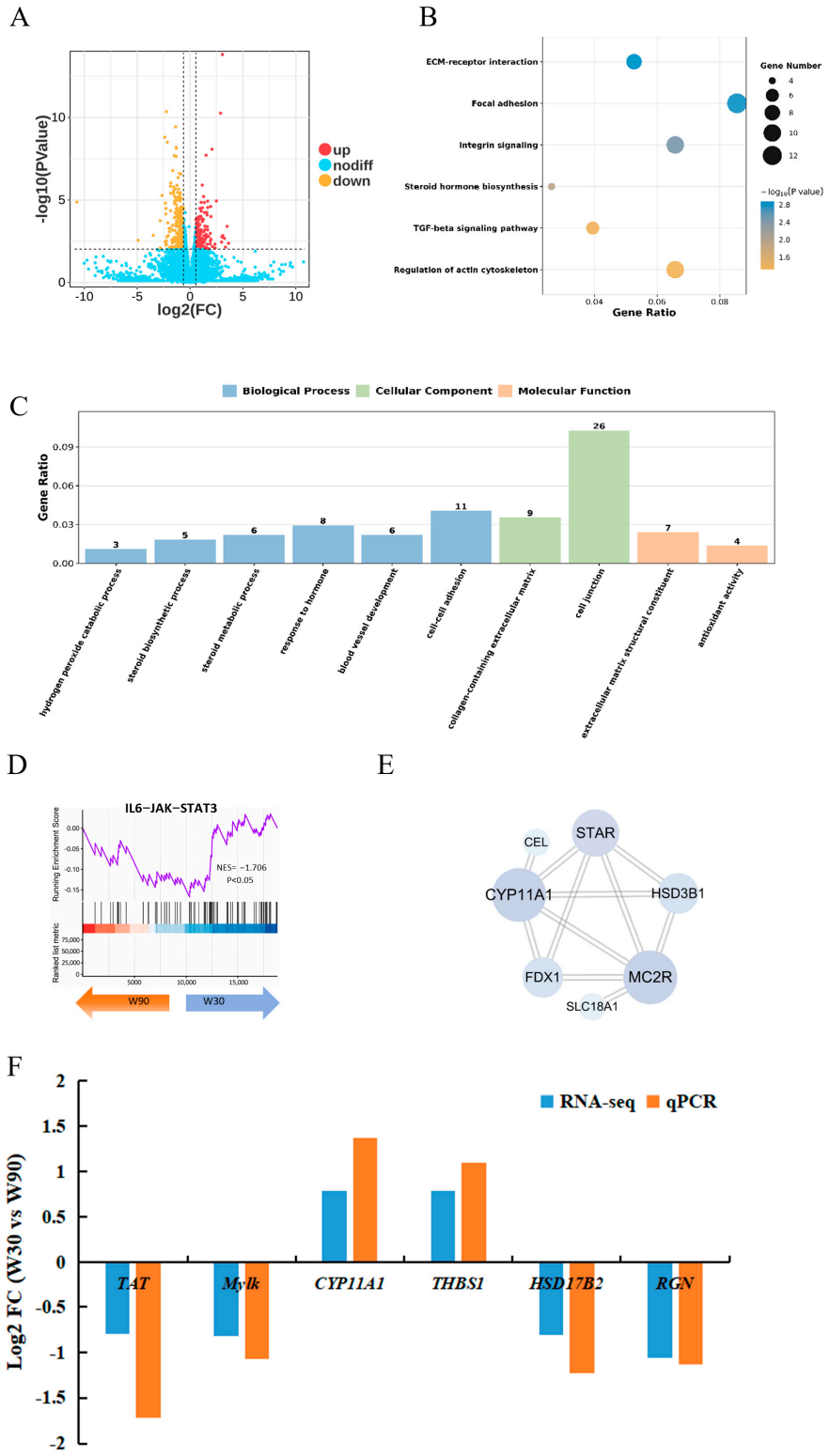


Figure 2. Transcriptional regulation associated with ovarian aging. (**A**) Volcano plot of DEGs between W90 and W30 ovaries. (**B**) KEGG pathway enrichment of DEGs. (**C**) GO enrichment of DEGs (BP, MF and CC categories). (**D**) GSEA of HALLMARK gene sets showing significant down-regulation of IL6-JAK-STAT3 signaling in W90. (**E**) PPI network of W90-down-regulated genes. (**F**) qRT-PCR validation of selected DEGs.

KEGG pathway analysis revealed that the DEGs between W30 and W90 ovaries were enriched in extracellular matrix-receptor interaction, focal adhesion, integrin signaling, steroid hormone biosynthesis, TGF-β signaling pathway, and regulation of the actin cytoskeleton (Figure 2B). GO enrichment analysis indicated that, in the biological process category, these DEGs were mainly associated with hydrogen peroxide catabolic process, steroid biosynthetic and metabolic processes, response to hormone, blood vessel development, and cell–cell adhesion. In the cellular component category, DEGs were enriched in collagen-containing extracellular matrix and cell junction, whereas molecular function terms included extracellular matrix structural constituent and antioxidant activity (Figure 2C).

GSEA of the HALLMARK gene sets indicated that only the HALLMARK_IL6_JAK_STAT3_SIGNALING pathway was significantly enriched and was down-regulated in W90 (Figure 2D). The PPI network constructed from W90-down-regulated genes identified a steroid synthesis-associated network (Figure 2E).

Six DEGs were selected for qRT-PCR validation. The qRT-PCR results were consistent with the RNA-seq data, confirming the reliability of the transcriptomic analysis (Figure 2F).

2.3. Translation Efficiency

Translational efficiency (TE) reflects the efficiency with which mRNAs are utilized by ribosomes and depends on both transcriptional and translational abundance. Correlation analysis showed positive correlations between mRNA levels and translation levels in both groups, with Pearson correlation coefficients of 0.6845 and 0.6538 for W90 and W30, indicating that genes with higher transcriptional levels generally exhibited higher translational output, respectively (Supplementary Figure S2).

The sequencing of each sample yielded between 10.07 and 11.64 million Ribo-seq clean reads, with reference genome alignment rates exceeding 87% (Supplementary Table S2). In conclusion, the results obtained from the RFs are deemed to be suitable for subsequent analysis. Subsequently, a total of 430 DTEGs were identified, including 338 down-regulated and 92 up-regulated genes, with down-regulated DTEGs being much more numerous than up-regulated ones in W90 (Figure 3A).

KEGG pathway analysis of differentially translated genes (DTEGs) revealed enrichment in focal adhesion, regulation of actin cytoskeleton, adherens junction, integrin signaling, ECM-receptor interaction, motor proteins, cell adhesion molecule interaction, and tight junction (Figure 3B). These pathways collectively indicate translational alterations related to extracellular matrix–cell interactions, cell adhesion and junctional organization, and cytoskeletal remodeling. GO enrichment analysis showed that, in the biological process category, DTEGs were mainly involved in the actin filament-based process, extracellular matrix, and regulation of intracellular signal transduction. In the cellular component category, DTEGs were enriched in stress fibers, extracellular matrix, extracellular space, and endoplasmic reticulum. Molecular function terms were mainly related to hormone binding, cell adhesion mediator activity, and calcium ion binding (Figure 3C).

The PPI network constructed from W90-up-regulated DTEGs revealed a core mechanical-stress remodeling module centered on *CAV1*, *MYL9*, *WASL*, *VWF* and WNT1 (Figure 3D).

2.4. Proteomic Analysis

To further investigate the key proteins associated with ovarian senescence in chickens, we performed DIA-based proteomic profiling. The results revealed the identification of 73,779 peptide segments, encompassing 6378 proteins (Supplementary Figure S3). Subsequently, 252 DEPs were screened, including 97 down-regulated and 155 up-regulated proteins in W90 (Figure 4A).

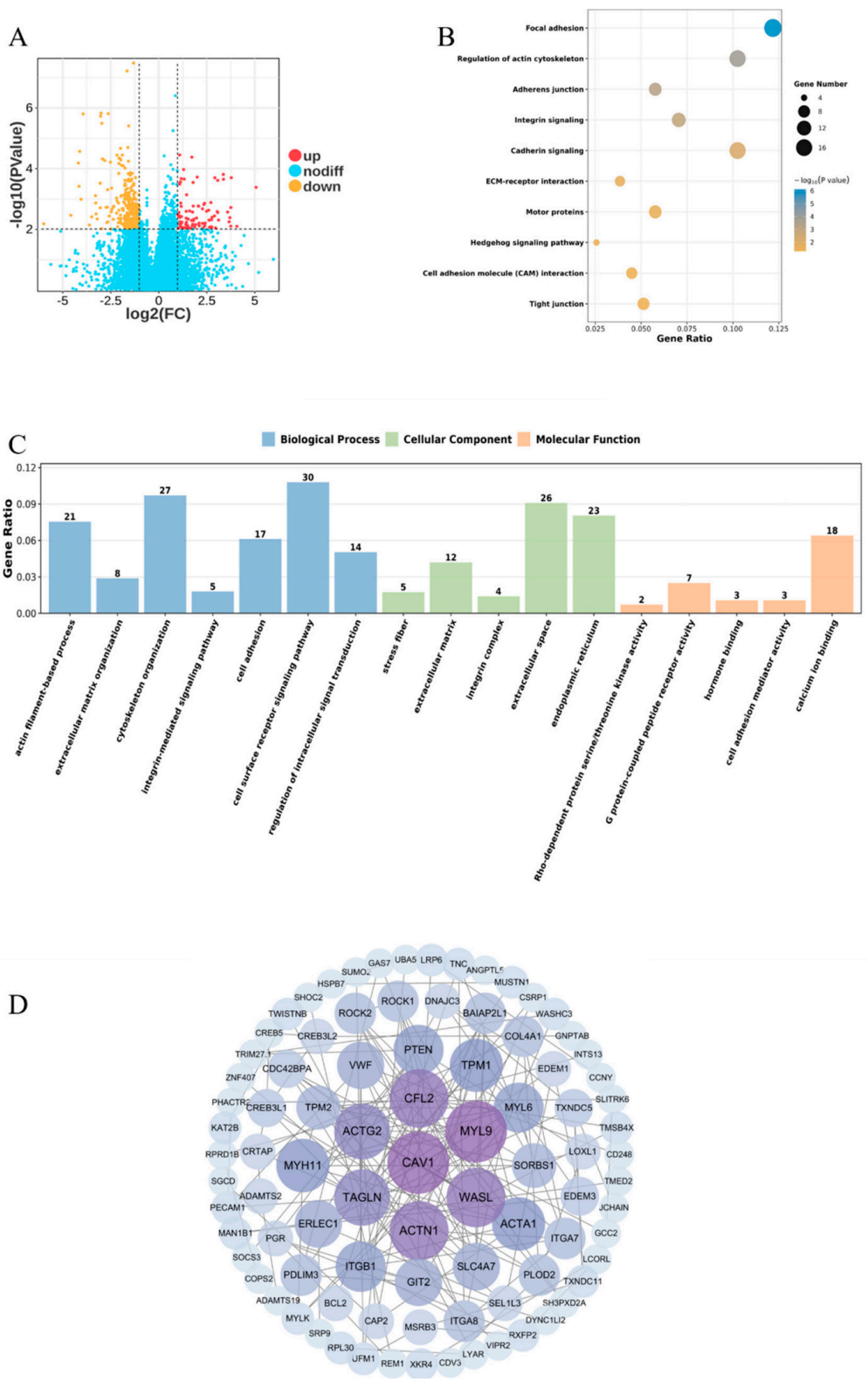


Figure 3. Translational efficiency–related regulation associated with ovarian aging. (**A**) Volcano plot of DTEGs between W90 and W30 ovaries. (**B**) KEGG enrichment of DTEGs. (**C**) GO enrichment of DTEGs. (**D**) PPI network of W90-up-regulated DTEGs, highlighting a mechanical-stress remodeling module.

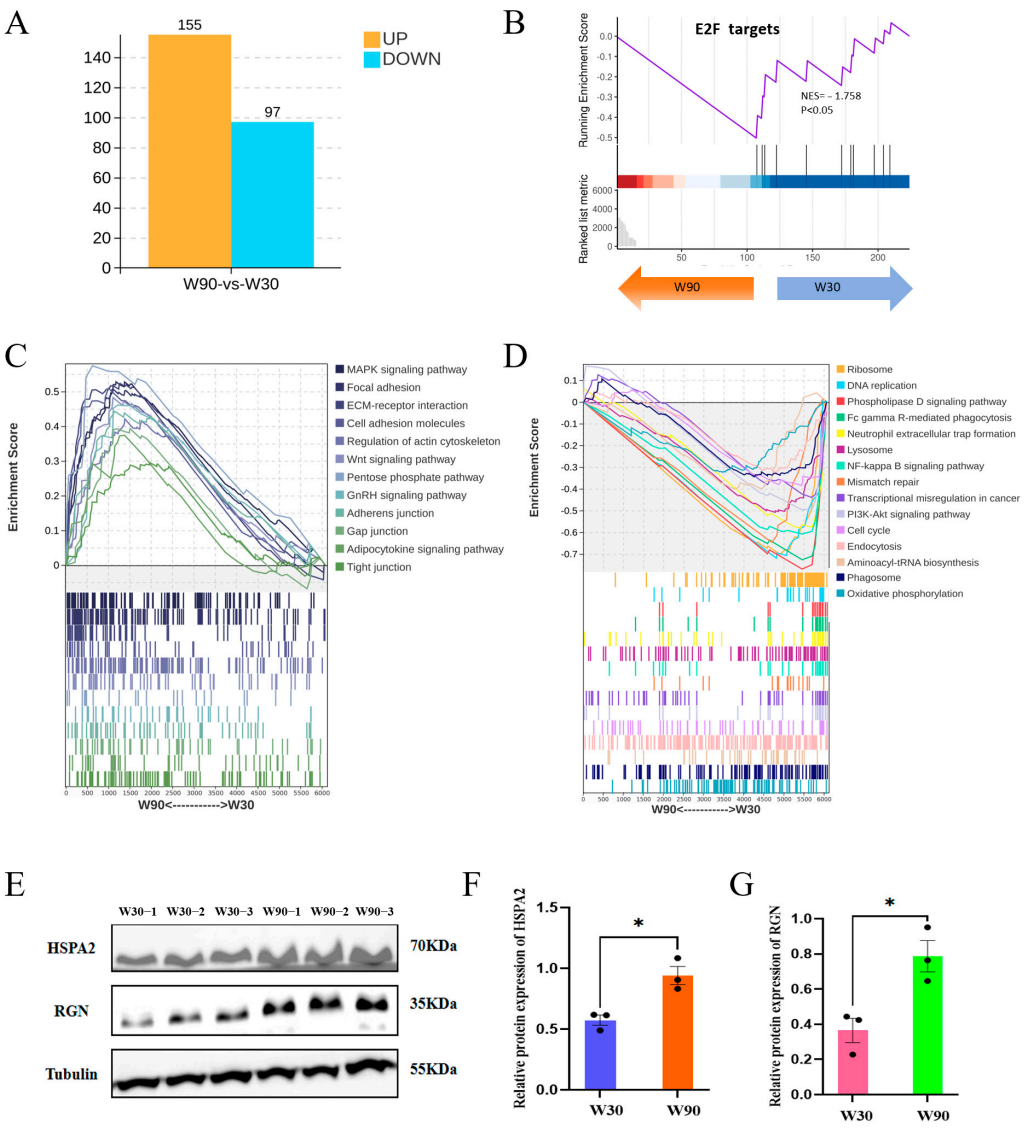


Figure 4. Proteomic changes associated with ovarian aging. (**A**) Number of DEPs between W90 and W30 ovaries. (**B**–**D**) GSEA of DEPs showing significantly down-regulated HALLMARK_E2F_TARGETS and differential regulation of multiple KEGG pathways. (**E**–**G**) Western blot validation of selected DEPs. * $p < 0.05$.

We then applied GSEA to the proteomic dataset. Specifically, HALLMARK analysis indicated that only the HALLMARK_E2F_TARGETS gene set was significantly enriched and down-regulated in W90 (Figure 4B). In contrast, W90 ovaries showed significant up-regulation of pathways such as MAPK, GnRH and Wnt signaling; ECM-receptor interaction; regulation of actin cytoskeleton; focal adhesion; cell adhesion molecules; adherens junction; tight junction; gap junction; pentose phosphate pathway; and adipocytokine signaling pathway (Figure 4C). Conversely, pathways including PI3K–Akt and NF-κB signaling, cell cycle, DNA replication, mismatch repair, oxidative phosphorylation, lysosome, phagosome, endocytosis, ribosome, aminoacyl-tRNA biosynthesis, transcriptional misregulation in cancer, Fc gamma R-mediated phagocytosis, neutrophil extracellular trap formation and phospholipase D signaling were significantly down-regulated in W90 (Figure 4D).

Two representative DEPs were validated by Western blotting. The protein abundance trends determined by Western blotting were consistent with those observed in the DIA proteomic data (Figure 4E–G).

2.5. Integrated Analysis of Transcriptome, Translation Efficiency and Proteome

To integrate the three omics layers, we first identified overlapping genes between any two of the transcriptome, TE and proteome datasets (Figure 5A). In total, 59 overlapping genes were detected.

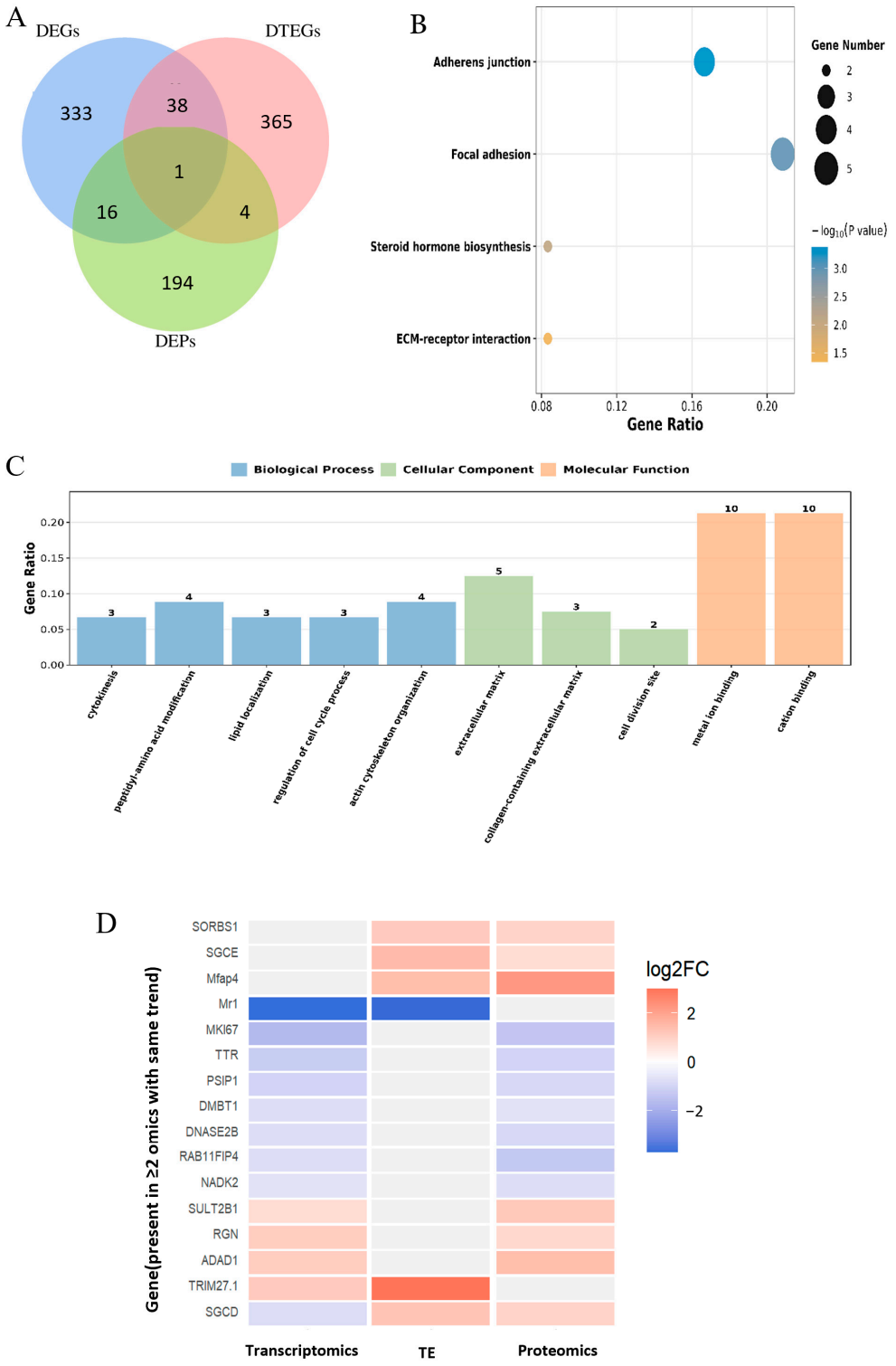


Figure 5. Integrated multi-omics analysis of ovarian aging. (**A**) Venn diagram of DEGs, DTEGs, and DEPs. (**B**) GO enrichment of the 59 overlapping genes. (**C**) KEGG enrichment of the 59 overlapping genes. (**D**) Heatmap of genes with consistent expression trends (up- or down-regulation) in at least two omics layers.

KEGG pathway analysis of the 59 genes differentially altered in at least two omics layers revealed enrichment in adherens junction, focal adhesion, steroid hormone biosynthesis, and ECM-receptor interaction (Figure 5B). GO enrichment analysis showed that, in the biological process category, these genes were mainly associated with cytokinesis, peptidyl-amino acid modification, and actin cytoskeleton organization. In the cellular component category, the enriched terms included collagen-containing extracellular matrix and cell division site, whereas metal ion binding and cation binding were enriched in the molecular function category (Figure 5C).

We then examined the expression trends of these 59 genes across the three omics levels. In most cases, transcript and TE trends were opposite. Genes that were down-regulated in both the transcriptome and proteome included PSIP1, MKI67, RAB11FIP4, TTR, NADK2 and DNASE2B, whereas genes up-regulated in both layers included ADAD1, RGN and SULT2B1. MFAP4, SGCE and SORBS1 were up-regulated in both TE and proteome datasets. Notably, SGCD showed decreased transcription but increased TE and protein abundance (Figure 5D).

3. Discussion

Egg-laying performance is a key economic trait in poultry production. Extending the effective laying period can reduce flock replacement costs and improve resource utilization efficiency. Ovarian aging may affect not only the number of follicles available for recruitment and ovulation, but also follicular competence and yolk deposition, thereby influencing both egg production and quality-related traits. Multi-omics investigations of ovarian aging in hens can facilitate the identification of key genes and pathways and provide a theoretical basis for developing future strategies to delay ovarian functional decline, maintain follicular viability, and prolong the laying period through nutritional interventions, genetic selection, and improved management practices.

Translomics aims to capture mRNA undergoing translation by ribosomes, closely linking with transcriptional regulation while reflecting the real-time output of protein synthesis [18]. Consequently, integrating translationalomics with transcriptomics and proteomics facilitates more precise identification of candidate molecules and their primary levels of change within the gene-translation-protein information flow framework, providing prioritised leads for subsequent validation. Combining three sets of omics data with experimental validation, this study identified key candidate genes and relevant biological processes involved in this process.

Steroidogenesis plays a central role in ovarian function and follicular development. The results of the present study indicate that genes involved in steroid hormone synthesis, such as *STAR*, *CYP11A1*, *HSD3B1*, and *FDX1*, are significantly down-regulated during ovarian aging (W90). Progesterone in avian species is mainly produced by granulosa cells of ovarian follicles, and its biosynthesis is synergistically regulated by multiple genes. *STAR* mediates the transport of cholesterol into mitochondria, which represents the rate-limiting step in steroidogenesis. Furthermore, *CYP11A1* and *HSD3B1* catalyze the conversion of cholesterol to progesterone, while *FDX1* directly participates in multiple enzymatic reactions converting cholesterol to sex hormones and acts as an essential cofactor for the activity of enzymes such as *CYP11A1* and *CYP17A1*. Previous studies have demonstrated that the expression of *STAR*, *CYP11A1* and *HSD3B* in chicken ovarian granulosa cells changes dynamically during folliculogenesis and correlates with alterations in progesterone secretion [19–23]. Moreover, integrated transcriptomic and single-cell transcriptomic analyses reveal that *FDX1* exhibits prominent promoter–enhancer interaction features at specific developmental stages, implying its involvement in follicular steroid synthesis [24].

In this study, signalling pathways associated with the extracellular matrix and intercellular interactions-namely, ECM-receptor interaction, Regulation of actin cytoskeleton, Focal adhesion, and Tight junction were found to be significantly up-regulated at W90. This finding was further corroborated by the protein interaction network of W90-up-regulated proteins. Specifically, genes associated with matrix fibrosis, such as MFAP4 and SGCE, were significantly up-regulated in both the translational efficiency and proteomic analyses. The extracellular matrix is a vital component of tissues, providing physical support and acting as a conduit for signal transduction. Fibrosis is widely recognised as one of the most prevalent aging-associated hallmarks and has been repeatedly demonstrated to induce structural disruption in tissues, thereby impairing organ biomechanics and function [1,25–28]. MFAP4 is a pivotal protein implicated in fibrotic processes during ECM remodelling [29,30]. SGCE participates in fibrosis by regulating FGF-BP1 [31–33].

Furthermore, it is imperative to acknowledge the pivotal roles that extracellular matrix degradation and clearance play in the processes of collagen deposition and ECM remodelling. The ovary of laying hens undergoes continuous and complex processes of follicle recruitment, development and ovulation. Enzymes including MMPs participate in stromal degradation to maintain the normal tissue architecture of the ovary [34]. A further exploration was conducted into the genes and pathways that regulate the clearance and degradation of the extracellular matrix. *ADAMTS15* [35], a matrix-associated metalloproteinase involved in proteoglycan cleavage and ECM remodelling, exhibited reduced expression in W90 ovaries. In a similar manner, *MRC1* [36], which is responsible for collagen internalisation and lysosomal degradation, was also found to be down-regulated. In our study, pathways associated with autophagy-lysosomal processes and clearance—including lysosomal, phagosomal, and endocytosis pathways involving CTSB and RAB7A proteins—demonstrated marked protein-level suppression. CTSB is a lysosomal cysteine protease that cleaves various proteins and extracellular matrix components, thereby participating in the regulation of autophagy within the body [37]. RAB7A plays a pivotal role in regulating endosome-lysosome transport and apoptotic autophagy processes [38]. Reduced levels of autophagy have been demonstrated across multiple species as hallmarks of aging [39–41]. As vital biological processes for cellular self-elimination, the down-regulation of autophagy degradation and apoptosis may constitute significant drivers of aging [42].

Collectively, these observations suggest that W90 ovaries undergo age-associated fibrotic ECM remodeling, potentially involving reduced matrix disassembly and impaired endocytic-autophagic clearance.

Within ovarian tissue, the process of aging has been shown to induce collagen deposition and alterations in key ECM components, such as hyaluronic acid. These changes have been associated with interstitial fibrosis and increased stiffness [43]. A study integrating extracellular matrix (ECM) proteomics and biomechanics also revealed that ovarian stromal cells acquire a more pronounced myofibroblastic phenotype during aging [28]. Selective reinforcement of the ECM leads to ovarian tissue stiffening, which impedes normal physiological processes such as follicular maintenance and ovulation. A study of transcriptomic and metabolomic profiles in 30-week-old and 80-week-old laying hens has revealed a decline in follicle numbers and an exacerbation of fibrosis in the ovaries of the older birds [44]. In contrast to the ovaries of mammals, the hen ovary facilitates frequent, continuous and hierarchical ovulation. Excessive ovarian stiffening has been demonstrated to directly interfere with follicle recruitment, rapid follicle expansion, follicle wall rupture and follicular atresia [45]. The proportional balance between follicles that successfully enter the preovulatory hierarchy and those undergoing atresia directly determines the laying performance of hens [46]. Concurrently, a stroma that has undergone fibrosis may impede accelerated follicle expansion. Follicles in the rapid growth phase undergo significant volume enlarge-

ment and require synchronised remodelling of the surrounding stroma. It is therefore hypothesised that excessive ECM retention or aberrant cell–matrix interactions may result in the restriction of follicle expansion. Accumulated ECM elevates the mechanical resistance of the follicle wall, leading to insufficient local tissue degradation and incomplete rupture of the preovulatory follicle. This has the potential to prolong ovulation intervals, increase the incidence of anovulation and follicular atresia, and ultimately result in decreased egg production. Furthermore, impaired follicular expansion and yolk deposition may alter yolk accumulation, egg weight, and the regularity of egg formation, thereby potentially affecting both egg production and egg quality.

Although integrated transcriptomic, translatomic and proteomic analyses offer a robust framework for screening candidate pathways, the present study has several limitations. First, three pooled biological replicates were used for omics analysis in each age group, which may weaken the capacity to resolve individual variation. Second, a set of candidate genes associated with ovarian aging was identified in this work, and their biological functions in vivo require further experimental validation.

4. Materials and Methods

4.1. Animals and Experimental Design

White Leghorn hens at 30 weeks of age (W30, peak laying stage, n = 6) and 90 weeks of age (W90, late laying stage, n = 6) were obtained from the Poultry Genetic Resources and Breeding Experimental Base of China Agricultural University. Ovarian tissues were collected from each hen approximately 12–14 h after egg laying, and follicles larger than 8 mm were removed. The samples were snap-frozen in liquid nitrogen and stored at −80 °C for subsequent omics analysis. Within each age group, samples from two hens were pooled to constitute one biological replicate, yielding three pooled biological replicates per age group. Body weight, ovarian weight, and the number of follicles ≥ 3 mm in diameter were recorded for each hen. Visible follicles were classified into three groups according to diameter: 3–5 mm, 6–8 mm, and >9 mm. The remaining follicles were evaluated using histological sections rather than being individually dissected. In this study, experimental chickens were euthanized via rapid carotid exsanguination. All animal experimental procedures complied with the Chinese national standard GB/T 35892-2018 [47] for the ethical review of laboratory animal welfare, and were approved on 8 February 2023 by the Committee of Laboratory Animal Welfare and Animal Experiment Ethics of China Agricultural University (License No.: AW80203202-1-1). Tissue collection was performed only after death was confirmed by complete cessation of respiration and heartbeat, together with the loss of physiological reflexes.

4.2. Paraffin Sectioning and Hematoxylin and Eosin (H&E) Staining of Ovarian Tissues

Ovarian tissues after removal of hierarchical follicles were fixed, embedded, and sectioned at a thickness of 5 μm. Following H&E staining, the sections were observed under a light microscope and imaged.

4.3. RNA Extraction and Sequencing

Total RNA was extracted from ovarian tissue using TRIzol reagent (Tiangen Biotech Co., Ltd., Beijing, China) for library construction. RNA integrity was assessed by 1% agarose gel electrophoresis and an Agilent 2100 Bioanalyzer, whereas RNA purity was determined using a NanoDrop 2000 spectrophotometer. Transcriptome library preparation and sequencing were performed by Gene Denovo Biotechnology Co., Ltd. (Guangzhou, China). mRNA libraries were constructed using the Hieff NGS® Ultima Dual-mode mRNA Library Prep Kit (Yeasen Biotechnology (Shanghai) Co., Ltd., Shanghai, China; Cat. No.

12309ES) according to the manufacturer's instructions. Non-strand-specific libraries were sequenced on an Illumina NovaSeq X Plus platform to generate 150 bp paired-end reads.

Raw sequencing reads were filtered using fastp (v0.18.0) [48] to obtain high-quality clean reads. Bowtie2 (v2.2.8) [49] was used to align the clean reads against an rRNA database, and reads mapped to rRNA sequences were discarded.

The chicken reference genome from Ensembl release 111 (https://ftp.ensembl.org/pub/release-111/fasta/gallus_gallus/dna/ (accessed on 1 September 2025)) was used as the reference genome. After construction of the genome index, the clean paired-end reads were aligned to the reference genome using HISAT2 (v2.1.0) with default parameters.

StringTie (v1.3.1) was used to reconstruct transcripts based on the uniquely mapped reads from each sample. RSEM [50] was used to calculate fragments per kilobase of transcript per million mapped reads (FPKM) values, which were subsequently used to calculate translation efficiency.

Differentially expressed genes (DEGs) between ovarian tissues from 30-week-old and 90-week-old hens were identified using DESeq2 (v1.24) [51] based on raw read counts. Genes with a fold change ≥ 1.5 or $\leq 1/1.5$ and p-value < 0.01 were considered differentially expressed. Kyoto Encyclopedia of Genes and Genomes (KEGG) pathway and Gene Ontology (GO) enrichment analyses of the DEGs were performed using KOBAS (http://bioinfo.org/kobas (accessed on 1 November 2025)). Protein–protein interactions were predicted using the STRING database, and the resulting interaction networks were visualized using Cytoscape (v3.10.1). In addition, gene set enrichment analysis (GSEA) of the complete gene set was performed using the LC-Bio Cloud Platform (https://www.omicstudio.cn/home (accessed on 5 November 2025)).

4.4. Ribosome Profiling Library Preparation and Sequencing

Ovarian tissue was thoroughly pulverized in liquid nitrogen. Ribosomes were isolated by gel-filtration chromatography, and RFs were recovered through sequential extraction and purification.

The resulting RFs were subjected to rRNA depletion. Ribosome profiling libraries were constructed using the NEBNext® Multiplex Small RNA Library Prep Set for Illumina® (New England Biolabs, Ipswich, MA, USA, Cat. Nos. E7300S and E7300L). Raw sequencing reads were quality-controlled and filtered using fastp (v0.20.0). First, qualified sequencing reads were aligned against the rRNA, GenBank and Rfam databases using Bowtie2 (v2.2.8). The remaining filtered reads were then mapped to the chicken reference genome (Ensembl release 111) with STAR (v2.5.1b) [52].

Raw read counts derived from the RNA-seq and ribosome profiling datasets were imported into RiboDiff to identify genes with altered translation efficiency. FPKM values were used to calculate translation efficiency for subsequent visualization according to the following formula: TE = Ribo-seq FPKM/RNA-seq FPKM [53]. Genes with a fold change ≥ 2 or ≤ 0.5 and p-value < 0.01 were defined as differentially translated genes (DTEGs).

4.5. DIA Proteomic Analysis

Ovarian tissues were lysed for protein extraction, and protein concentration was determined using the Pierce™ Rapid Gold BCA Protein Assay Kit (Thermo Fisher Scientific, Waltham, MA, USA, Cat. No. A53225).

The desalted and vacuum-dried peptides were reconstituted in mobile phase A, consisting of 0.1% formic acid in water, and subjected to LC-MS/MS analysis using a timsTOF Pro 2 mass spectrometer (Bruker Daltonik, Bremen, Germany) coupled to an UltiMate 3000 system (Thermo Fisher Scientific, Waltham, MA, USA). The DIA raw data were analyzed

using Spectronaut 18 with the default BGS Factory Settings. Peptides passing the 1.0% FDR threshold were used for protein-group quantification using the MaxLFQ algorithm.

Statistical analyses were performed using R software(v4.5.1). An independent-samples *t*-test was used to compare protein abundance between the 90-week-old (W90) and 30-week-old (W30) groups. Proteins with a fold change ≥ 1.5 or ≤1/1.5 and *p*-value < 0.01 were defined as differentially expressed proteins (DEPs).

4.6. Real-Time Quantitative PCR

To validate the RNA-seq results, six differentially expressed genes (DEGs) were selected for quantitative real-time PCR (qRT-PCR) analysis. The same RNA samples used for RNA-seq were reverse-transcribed into complementary DNA (cDNA) using the FastQuant RT Kit with gDNA Eraser (Tiangen Biochemical Technology Co., Ltd., Beijing, China) according to the manufacturer's instructions. Primers were designed using the NCBI Primer-BLAST tool (https://www.ncbi.nlm.nih.gov/tools/primer-blast/ (accessed on 16 November 2025)), and the primer sequences are listed in Supplementary Table S3.

Amplification efficiency was validated by standard curves generated from 5-fold serial dilutions of cDNA template (five concentration points). Only assays with amplification efficiency between 90% and 110% and $R^2 > 0.99$ were accepted. Three biological replicates were included per group, and each biological replicate was run in triplicate as technical replicates. qRT-PCR was performed using SYBR Green PCR Master Mix from Tiangen. Each reaction was conducted in a total volume of 20 µL containing 1 µL of cDNA template, 10 µL of 2× qPCR Pre-Mix, 0.6 µL of each forward and reverse primer, and 7.8 µL of RNase-free water. The thermal cycling conditions were as follows: initial denaturation at 95 °C for 3 min, followed by 40 cycles of denaturation at 95 °C for 5 s, annealing at 60 °C for 10 s, and extension at 72 °C for 15 s. Relative gene expression levels were calculated using the $2^{-\Delta\Delta Ct}$ method [54], with β-actin used as the reference gene.

4.7. Western Blotting

Protein concentrations were determined using a BCA protein assay kit (Shanghai Biyuntian Biotechnology Co., Ltd., Shanghai, China). Proteins were separated on SDS-PAGE gels of appropriate acrylamide concentration, depending on the molecular weight, and then transferred onto PVDF membranes (Bio-Rad Laboratories, Inc., Hercules, CA, USA) pre-activated in methanol. Membranes were blocked and incubated overnight at 4 °C with specific primary antibodies. After washing, membranes were incubated with corresponding HRP-conjugated secondary antibodies for 1 h at room temperature. Signals were visualized using an ECL reagent, and band intensities were quantified with ImageJ (v1.54) software. Details of the antibodies used are provided in Supplementary Table S4.

4.8. Statistical Analysis

Statistical analysis of gene, protein validation, and phenotypic measurements was performed using SPSS 25.0 (SPSS Inc., Chicago, IL, USA). At least three independent biological replicates were included for each comparison. Differences between W30 and W90 groups were evaluated using independent-samples *t*-tests. Data are presented as mean ± standard error of the mean (SEM). A *p*-value < 0.05 is considered statistically significant, with *p*-values < 0.01 indicating a highly significant difference.

5. Conclusions

In conclusion, our research uses complementary multi-omics data to create a relatively comprehensive map of ovarian aging at pathway and gene levels. Our results indicate that ovarian ageing in chickens is characterized by diminished hormone synthesis and

ovarian structural remodeling. Eventually, this process contributes to progressive ovarian functional decline and exhaustion of the follicle reserve. By deciphering molecular changes underlying ovarian aging in laying hens, this study lays a theoretical foundation for further related investigations.

Supplementary Materials: The following supporting information can be downloaded at https://www.mdpi.com/article/10.3390/ijms272210421/s1.

Author Contributions: W.M. and A.G. analysed the data and wrote the article; S.H., H.Z. (Hongliang Zhang) and W.Z. collected and verified the samples. B.Z. and H.Z. (Hao Zhang) provided suggestions on our article and assistance with grammatical writing. All authors have read and agreed to the published version of the manuscript.

Funding: This study was supported by Key R&D Program of Shandong Province, China: Agricultural Breed Project of Shandong Province (Grant No. 2025LZGC048), Chinese Universities Scientific Fund (2025TC135, 2025TC067), and China Agriculture Research System (CARS-39-K05).

Institutional Review Board Statement: The animal study protocol was approved by the Committee of Laboratory Animal Welfare and Animal Experiment Ethics of China Agricultural University (protocol code: AW80203202-1-1; date of approval: 8 February 2023). All chickens were raised under equivalent environmental conditions, and feed and water were provided ad libitum. In the interest of animal welfare, all animals were slaughtered humanely, and all efforts were made to minimize suffering.

Informed Consent Statement: Not applicable.

Data Availability Statement: The data for the current study are available from the corresponding author upon reasonable request. The RNA-seq data and translatome data generated in this study have been deposited in the NCBI Sequence Read Archive (SRA) under the accession numbers PRJNA1404638 and PRJNA1404880, respectively. The mass spectrometry proteomics data have been deposited to the ProteomeXchange Consortium via the iProX partner repository (https://proteomecentral.proteomexchange.org (accessed on 20 November 2025)) with the dataset identifier PXD073314.

Conflicts of Interest: The authors declare no conflicts of interest.

Abbreviations

The following abbreviations are used in this manuscript:

DEGs	Differentially Expressed Genes
DTEGs	Differentially Translated Genes
DEPs	Differentially Expressed Proteins
KEGG	Kyoto Encyclopedia of Genes and Genomes
TE	Translational efficiency
FDR	False Discovery Rate
DIA	Data-independent AECMcquisition
qRT-PCR	quantitative real-time PCR
ECM	Extracellular Matrix

References

1. Umehara, T.; Winstanley, Y.E.; Andreas, E.; Morimoto, A.; Williams, E.J.; Smith, K.M.; Carroll, J.; Febbraio, M.A.; Shimada, M.; Russell, D.L.; et al. Female reproductive life span is extended by targeted removal of fibrotic collagen from the mouse ovary. *Sci. Adv.* **2022**, *8*, e4564. [CrossRef] [PubMed]
2. Wang, X.; Wang, L.; Xiang, W. Mechanisms of ovarian aging in women: A review. *J. Ovarian Res.* **2023**, *16*, 67. [CrossRef] [PubMed]
3. Wang, S.; Zheng, Y.; Li, J.; Yu, Y.; Zhang, W.; Song, M.; Liu, Z.; Min, Z.; Hu, H.; Jing, Y.; et al. Single-cell transcriptomic atlas of primate ovarian aging. *Cell* **2020**, *180*, 585–600. [CrossRef] [PubMed]
4. Pei, L.; Wang, W.; Guo, P.; Qiao, A.; Duan, X.; Xu, X.; Liu, C. Integrated analysis of differential m6A methylation and transcriptome profiles in ovaries of young and aged Qira black sheep. *BMC Genom.* **2026**, *27*, 251. [CrossRef] [PubMed]

5. Senbeta, E.K. Performance of white leghorn chickens breed maintained at haramaya university poultry farm and implications for sustainable poultry production. *East. Afr. J. Sci.* **2020**, *14*, 13–22. Available online: https://eajs.haramayajournals.org/index.php/eajs/article/view/974 (accessed on 1 September 2025).
6. Shi, J.; Xiong, H.; Su, J.; Wang, Q.; Wang, H.; Yang, C.; Hu, C.; Cui, Z.; Liu, L. Multiomics analyses reveal high yield-related genes in the hypothalamic-pituitary-ovarian/liver axis of chicken. *Poult. Sci.* **2024**, *103*, 104276. [CrossRef] [PubMed]
7. Leng, D.; Zeng, B.; Wang, T.; Chen, B.; Li, D.; Li, Z. Single nucleus/cell RNA-seq of the chicken hypothalamic-pituitary-ovarian axis offers new insights into the molecular regulatory mechanisms of ovarian development. *Zool. Res.* **2024**, *45*, 1088–1107. [CrossRef] [PubMed]
8. Yang, Q.; Chen, W.; Cong, L.; Wang, M.; Li, H.; Wang, H.; Luo, X.; Zhu, L.; Zeng, X.; Zhu, Z.; et al. NADase CD38 is a key determinant of ovarian aging. *Nat. Aging* **2024**, *4*, 110–128. [CrossRef] [PubMed]
9. Molnár, A.; Maertens, L.; Ampe, B.; Buyse, J.; Kempen, I.; Zoons, J.; Delezie, E. Changes in egg quality traits during the last phase of production: Is there potential for an extended laying cycle? *Br. Poult. Sci.* **2016**, *57*, 842–847. [CrossRef] [PubMed]
10. Thiruvenkadan, A.K.; Panneerselvam, S.; Prabakaran, R. Layer breeding strategies: An overview. *Worlds Poult. Sci. J.* **2010**, *66*, 477–502. [CrossRef]
11. Alo, E.T.; Daramola, J.O.; Wheto, M.; Oke, O.E. Impact of broiler breeder hens' age and egg storage on egg quality, embryonic development, and hatching traits of FUNAAB-alpha chickens. *Poult. Sci.* **2024**, *103*, 103313. [CrossRef] [PubMed]
12. Zhou, H.; Clark, E.; Guan, D.; Lagarrigue, S.; Fang, L.; Cheng, H.; Tuggle, C.K.; Kapus, M.; Wang, Y.; Giuffra, E.; et al. Comparative genomics and epigenomics of transcriptional regulation. *Annu. Rev. Anim. Biosci.* **2025**, *13*, 73–98. [CrossRef] [PubMed]
13. Jaswal, S.; Anand, V.; Ali, S.A.; Jena, M.K.; Kumar, S.; Kaushik, J.K.; Mohanty, A.K. TMT based deep proteome analysis of buffalo mammary epithelial cells and identification of novel protein signatures during lactogenic differentiation. *FASEB J.* **2021**, *35*, e2162. [CrossRef] [PubMed]
14. Xu, Y.; Zhang, Y.; Qin, Y.; Gu, M.; Chen, R.; Sun, Y.; Wu, Y.; Li, Q.; Qiao, Y.; Wang, X.; et al. Multi-omics analysis of functional substances and expression verification in cashmere fineness. *BMC Genom.* **2023**, *24*, 720. [CrossRef] [PubMed]
15. Solyga, M.; Majumdar, A.; Besse, F. Regulating translation in aging: From global to gene-specific mechanisms. *EMBO Rep.* **2024**, *25*, 5265–5276. [CrossRef] [PubMed]
16. Chai, R.; Xiao, C.; Yang, Z.; Du, W.; Lv, K.; Zhang, J.; Yang, X. Identification of genes associated with sperm storage capacity in hens at different times after insemination by RNA-seq and Ribo-seq. *BMC Genom.* **2024**, *25*, 554. [CrossRef] [PubMed]
17. Huang, J.; Chen, P.; Jia, L.; Li, T.; Yang, X.; Liang, Q.; Zeng, Y.; Liu, J.; Wu, T.; Hu, W.; et al. Multi-Omics analysis reveals translational landscapes and regulations in mouse and human oocyte aging. *Adv. Sci.* **2023**, *10*, e2301538. [CrossRef] [PubMed]
18. King, H.A.; Gerber, A.P. Translatome profiling: Methods for genome-scale analysis of mRNA translation. *Brief. Funct. Genom.* **2016**, *15*, 22–31. [CrossRef] [PubMed]
19. Ma, X.; Han, X.; Zhang, Q.; Wang, W.; Tang, H. Synergistic cooperation between the β-catenin and SF1 regulates progesterone synthesis in laying hen ovarian granulosa cells. *Anim. Biotechnol.* **2024**, *35*, 2351975. [CrossRef] [PubMed]
20. Xu, Q.; Song, Y.; Chen, Y.; Liu, R.; Zhang, Y.; Li, Y.; Huang, Z.; Zhao, W.; Chang, G.; Chen, G. Molecular cloning and expression patterns of the cholesterol side chain cleavage enzyme (CYP11A1) gene during the reproductive cycle in goose (*Anas cygnoides*). *J. Anim. Sci. Biotechnol.* **2015**, *6*, 54. [CrossRef] [PubMed]
21. Sechman, A.; Pawlowska, K.; Hrabia, A. Effect of 3,3′,5-triiodothyronine and 3,5-diiodothyronine on progesterone production, cAMP synthesis, and mRNA expression of STAR, CYP11A1, and HSD3B genes in granulosa layer of chicken preovulatory follicles. *Domest. Anim. Endocrinol.* **2011**, *3*, 137–149. [CrossRef] [PubMed]
22. Li, J.; Luo, W.; Huang, T.; Gong, Y. Growth differentiation factor 9 promotes follicle-stimulating hormone-induced progesterone production in chicken follicular granulosa cells. *Gen. Comp. Endocrinol.* **2019**, *276*, 69–76. [CrossRef] [PubMed]
23. Wan, E.; Zhu, W.; Wang, C.; Li, J.; Fan, X.; Miao, Y. Spatiotemporal expression inversion of cyp11a1 in the hpo axis and its regulation of granulosa cell proliferation via the PI3K/AKT/mTOR pathway in wuding chickens. *Animals* **2026**, *16*, 657. [CrossRef] [PubMed]
24. Li, D.; Ning, C.; Zhang, J.; Wang, Y.; Tang, Q.; Kui, H.; Wang, T.; He, M.; Jin, L.; Li, J.; et al. Dynamic transcriptome and chromatin architecture in granulosa cells during chicken folliculogenesis. *Nat. Commun.* **2022**, *13*, 131. [CrossRef] [PubMed]
25. Chen, K.; Ma, J.; Jia, X.; Ai, W.; Ma, Z.; Pan, Q. Advancing the understanding of NAFLD to hepatocellular carcinoma development: From experimental models to humans. *Biochim. Biophys. Acta Rev. Cancer* **2019**, *1871*, 117–125. [CrossRef] [PubMed]
26. Giménez, A.; Duch, P.; Puig, M.; Gabasa, M.; Xaubet, A.; Alcaraz, J. Dysregulated collagen homeostasis by matrix stiffening and TGF-β1 in fibroblasts from idiopathic pulmonary fibrosis patients: Role of FAK/Akt. *Int. J. Mol. Sci.* **2017**, *18*, 2431. [CrossRef] [PubMed]
27. McCloskey, C.W.; Cook, D.P.; Kelly, B.S.; Azzi, F.; Allen, C.H.; Forsyth, A.; Upham, J.; Rayner, K.J.; Gray, D.A.; Boyd, R.W.; et al. Metformin abrogates age-associated ovarian fibrosis. *Clin. Cancer Res.* **2020**, *26*, 632–642. [CrossRef] [PubMed]

28. Amargant, F.; Manuel, S.L.; Tu, Q.; Parkes, W.S.; Rivas, F.; Zhou, L.T.; Rowley, J.E.; Villanueva, C.E.; Hornick, J.E.; Shekhawat, G.S.; et al. Ovarian stiffness increases with age in the mammalian ovary and depends on collagen and hyaluronan matrices. *Aging Cell* **2020**, *19*, e13259. [CrossRef] [PubMed]
29. Pan, Z.; Yang, K.; Wang, H.; Xiao, Y.; Zhang, M.; Yu, X.; Xu, T.; Bai, T.; Zhu, H. MFAP4 deficiency alleviates renal fibrosis through inhibition of NF-κB and TGF-β/Smad signaling pathways. *FASEB J.* **2020**, *34*, 14250–14263. [CrossRef] [PubMed]
30. Liu, L.; Li, B.; Zhang, Y.; Nie, Y.; Zhang, W.; Chen, P.; Huang, C.; Zhu, X. MFAP4 deficiency attenuates liver fibrosis by regulating hepatic stellate cell fate through inhibition of the FAK/PI3K/NFκB signaling pathway. *Cell Mol. Gastroenterol. Hepatol.* **2025**, *19*, 101548. [CrossRef] [PubMed]
31. Qiu, T.; Hou, L.; Zhao, L.; Wang, X.; Zhou, Z.; Yang, C.; Zhang, H.; Jiang, D.; Jiao, B.; Chen, C. SGCE promotes breast cancer stemness by promoting the transcription of FGF-BP1 by Sp1. *J. Biol. Chem.* **2023**, *299*, 105351. [CrossRef] [PubMed]
32. Wang, D.; Eraslan, B.; Wieland, T.; Hallström, B.; Hopf, T.; Zolg, D.P.; Zecha, J.; Asplund, A.; Li, L.; Meng, C.; et al. A deep proteome and transcriptome abundance atlas of 29 healthy human tissues. *Mol. Syst. Biol.* **2019**, *15*, e8503. [CrossRef] [PubMed]
33. Keele, G.R.; Zhang, J.G.; Szpyt, J.; Korstanje, R.; Gygi, S.P.; Churchill, G.A.; Schweppe, D.K. Global and tissue-specific aging effects on murine proteomes. *Cell Rep.* **2023**, *42*, 112715. [CrossRef] [PubMed]
34. Hrabia, A. Matrix metalloproteinases (MMPs) and inhibitors of MMPs in the avian reproductive system: An overview. *Int. J. Mol. Sci.* **2021**, *22*, 8056. [CrossRef] [PubMed]
35. Kelwick, R.; Desanlis, I.; Wheeler, G.N.; Edwards, D.R. The ADAMTS (A Disintegrin and Metalloproteinase with Thrombospondin motifs) family. *Genome Biol.* **2015**, *16*, 113. [CrossRef] [PubMed]
36. Madsen, D.H.; Leonard, D.; Masedunskas, A.; Moyer, A.; Jessen, H.J.; Peters, D.E.; Amornphimoltham, P.; Selvaraj, A.; Yamada, S.S.; Brenner, D.A.; et al. M2-like macrophages are responsible for collagen degradation through a mannose receptor-mediated pathway. *J. Cell Biol.* **2013**, *202*, 951–966. [CrossRef] [PubMed]
37. Mohanty, A.; Kumari, A.; Kumar, L.; Kumar, A.; Birajdar, P.; Beniwal, R.; Athar, M.; Kumar, K.; Rao, H.B.D.P. Cathepsin b regulates ovarian reserve quality and quantity via mitophagy by modulating IGF1R turnover. *Aging Cell* **2025**, *24*, e70066. [CrossRef] [PubMed]
38. Liu, W.; Wang, K.; Lin, Y.; Wang, L.; Jin, X.; Qiu, Y.; Sun, W.; Zhang, L.; Sun, Y.; Dou, X.; et al. VPS34 governs oocyte developmental competence by regulating mito/autophagy: A novel insight into the significance of RAB7 activity and its subcellular location. *Adv. Sci.* **2024**, *11*, e2308823. [CrossRef] [PubMed]
39. Minami, S.; Yamamoto, T.; Yamamoto-Imoto, H.; Isaka, Y.; Hamasaki, M. Autophagy and kidney aging. *Prog. Biophys. Mol. Biol.* **2023**, *179*, 10–15. [CrossRef] [PubMed]
40. Aman, Y.; Schmauck-Medina, T.; Hansen, M.; Morimoto, R.I.; Simon, A.K.; Bjedov, I.; Palikaras, K.; Simonsen, A.; Johansen, T.; Tavernarakis, N.; et al. Autophagy in healthy aging and disease. *Nat. Aging* **2021**, *1*, 634–650. [CrossRef] [PubMed]
41. Palmer, J.E.; Wilson, N.; Son, S.M.; Obrocki, P.; Wrobel, L.; Rob, M.; Takla, M.; Korolchuk, V.I.; Rubinsztein, D.C. Autophagy, aging, and age-related neurodegeneration. *Neuron* **2025**, *113*, 29–48. [CrossRef] [PubMed]
42. Baxi, K.; Ghavidel, A.; Waddell, B.; Harkness, T.A.; de Carvalho, C.E. Regulation of lysosomal function by the DAF-16 forkhead transcription factor couples reproduction to aging in caenorhabditis elegans. *Genetics* **2017**, *207*, 83–101. [CrossRef] [PubMed]
43. Pennarossa, G.; Iorio, T.D.; Gandolfi, F.; Brevini, T.A.L. Impact of aging on the ovarian extracellular matrix and derived 3D scaffolds. *Nanomaterials* **2022**, *12*, 345. [CrossRef] [PubMed]
44. He, H.; Ma, Q.; Zhang, X.; Zhou, C.; Liu, F.; Lu, Y.; Yu, M. Integrated analysis of transcriptome and metabolomic uncover molecular mechanisms of ovarian aging in laying hens. *Poult. Sci.* **2026**, *105*, 106811. [CrossRef] [PubMed]
45. Ghanem, K.; Johnson, A.L. Relationship between cyclic follicle recruitment and ovulation in the hen ovary. *Poult. Sci.* **2019**, *98*, 3014–3021. [CrossRef] [PubMed]
46. Poudel, S.; Khadka, V.S.; Jha, R.; Mishra, B. Age-related changes in the transcriptomic profile associated with ovarian small white follicle recruitment in commercial laying hens. *Poult. Sci.* **2026**, *105*, 106057. [CrossRef] [PubMed]
47. *GB/T 35892-2018*; Laboratory Animal—Guideline for Ethical Review of Animal Welfare. Standardization administration of China: Beijing, China, 2018. Available online: https://openstd.samr.gov.cn/bzgk/std/newGbInfo?hcno=9BA619057D5C13103622A10FF4BA5D14 (accessed on 16 November 2025).
48. Chen, S.; Zhou, Y.; Chen, Y.; Gu, J. fastp: An ultra-fast all-in-one FASTQ preprocessor. *Bioinformatics* **2018**, *17*, i884–i890. [CrossRef] [PubMed]
49. Langmead, B.; Salzberg, S.L. Fast gapped-read alignment with Bowtie 2. *Nat. Methods* **2012**, *9*, 357–359. [CrossRef] [PubMed]
50. Li, B.; Dewey, C.N. RSEM: Accurate transcript quantification from RNA-Seq data with or without a reference genome. *BMC Bioinform.* **2011**, *1*, 323. [CrossRef] [PubMed]
51. Love, M.I.; Huber, W.; Anders, S. Moderated estimation of fold change and dispersion for RNA-seq data with DESeq2. *Genome Biol.* **2014**, *15*, 550. [CrossRef] [PubMed]
52. Dobin, A.; Davis, C.A.; Schlesinger, F.; Drenkow, J.; Zaleski, C.; Jha, S.; Batut, P.; Chaisson, M.; Gingeras, T.R. STAR: Ultrafast universal RNA-seq aligner. *Bioinformatics* **2013**, *29*, 15–21. [CrossRef] [PubMed]

53. Ingolia, N.T.; Ghaemmaghami, S.; Newman, J.R.S.; Weissman, J.S. Genome-wide analysis in vivo of translation with nucleotide resolution using ribosome profiling. *Science* **2009**, *324*, 218–223. [CrossRef] [PubMed]
54. Livak, K.J.; Schmittgen, T.D. Analysis of relative gene expression data using real-time quantitative PCR and the 2(-Delta Delta C(T)) Method. *Methods* **2001**, *4*, 402–408. [CrossRef] [PubMed]

Disclaimer/Publisher's Note: The statements, opinions and data contained in all publications are solely those of the individual author(s) and contributor(s) and not of MDPI and/or the editor(s). MDPI and/or the editor(s) disclaim responsibility for any injury to people or property resulting from any ideas, methods, instructions or products referred to in the content.